Electrocatalysis

Space-Confinement-Induced Synthesis of Pyridinic- and Pyrrolic-Nitrogen-Doped Graphene for the Catalysis of Oxygen Reduction**

Wei Ding, Zidong Wei, Siguo Chen, Xueqiang Qi, Tao Yang, Jinsong Hu, Dong Wang,*
Li-Jun Wan, Shahnaz Fatima Alvi, and Li Li*

The development of high-performance and low-cost catalytic materials for the oxygen reduction reaction (ORR) has been a major challenge for the large-scale application of fuel cells.[1] Currently, platinum and platinum-based alloys are the most efficient ORR catalysts in fuel-cell cathodes;[2] however, they cannot meet the demand for the widespread commercialization of fuel cells because of the scarcity of platinum. Thus, the ongoing search for platinum-free catalysts for the ORR has attracted much attention. Graphene, single-layer sheets of sp^2-hybridized carbon atoms, has attracted tremendous attention and research interest.[3] The abundance of free-flowing π electrons in carbon materials composed of sp^2-hybridized carbon atoms makes these materials potential catalysts for reactions that require electrons, such as the ORR. However, these π electrons are too inert to be used directly in the ORR. In N-doped electron-rich carbon nanostructures, carbon π electrons have been shown to be activated through conjugation with lone-pair electrons from N dopants; thus, O_2 molecules are reduced on the positively charged C atoms that neighbor N atoms.[1a,4] Recently, Hu and co-workers found that as long as the electroneutrality of the sp^2-hybridized carbon atoms is broken and charged sites that favor O_2 adsorption are created, these materials will be transformed into active metal-free ORR electrocatalysts regardless of whether the dopants are electron-rich (e.g., N) or electron-deficient (e.g., B).[5] Nitrogen-doped carbon (NC) materials are considered to be promising catalysts because of their acceptable ORR activity, low cost, good durability, and environmental friendliness.[1a,4a,6] However, their ORR activity is less competitive, especially in acidic media. Relative to commercial Pt/C, the difference in the half-wave potential for

ORR is within 25 mV in alkaline electrolytes but is greater than 200 mV in acidic electrolytes.[4a,6] The activity of NC materials can be enhanced through efficient N doping with sufficient active species that favor ORR and through an increase in electrical conductivity.[1a,7]

The annealing of graphitized carbon materials, such as carbon nanotubes[8a,b] and microporous carbon black,[4b,8c] in NH_3 leads to insufficient substitution of nitrogen because of the well-ordered structure of the host materials.[1b] Alternatively, the direct pyrolysis of nitrogen-containing hydrocarbons or polymers produces NC materials with good incorporation of nitrogen.[4a,9] However, suitable pyrolysis temperatures are difficult to pinpoint; without optimization, temperatures that are excessively low or excessively high lead to low electronic conductivity or a remarkable loss of active N species, respectively.[10]

Recently, mesoporous-alumina-assisted and silica-template-assisted nitrogen incorporation, which can preserve a high content of N in synthesized NC materials, have been reported.[11] However the activities of the resulting NC materials in the ORR were still significantly lower than that of Pt/C, even when the N content was as high as 10.7 atm%.[12a] Among three types of N atoms, that is, pyridinic, pyrrolic, and quaternary N, only the pyridinic and pyrrolic forms, which have planar structures, have been proven to be active in the ORR.[4a,7,11] In contrast, quaternary N atoms, which possess a 3D structure, are not active in the ORR. The low electrical conductivity of NC materials with quaternary N atoms results from the interruption of their π–π conjugation by the 3D structure and is thought to be predominantly responsible for the poor catalysis.[12] Therefore, the synthesis of NC materials with more planar pyridinic and pyrrolic N atoms and fewer quaternary N atoms is important for the preparation of ORR-active catalysts.

Herein, we present a novel strategy for the selective synthesis of pyridinic- and pyrrolic-nitrogen-doped graphene (NG) by the use of layered montmorillonite (MMT) as a quasi-closed flat nanoreactor, which is open only along the perimeter to enable the entrance of aniline (AN) monomer molecules. The flat MMT nanoreactor, which is less than 1 nm thick, extensively constrains the formation of quaternary N because of its 3D structure but facilitates the formation of pyridinic and pyrrolic N. Nitrogen is well-known to be incorporated into quaternary N in tetrahedral sp^3 hybridization but incorporated into pyridinic and pyrrolic N in planar sp^2 hybridization.[13] The confinement effect of MMT ensures that N is incorporated into the structure and that the graphitization is successful without significant loss of N species. Furthermore, planar pyridinic and pyrrolic N can be

[*] Dr. W. Ding, Prof. Z.-D. Wei, Dr. S.-G. Chen, Dr. X.-Q. Qi, Dr. T. Yang, Dr. S. F. Alvi, Dr. L. Li
The State Key Laboratory of Power Transmission Equipment and System Security and New Technology, College of Chemistry and Chemical Engineering, Chongqing University
Shapingba 174, Chongqing (China)
E-mail: zdwei@cqu.edu.cn

Prof. J.-S. Hu, Prof. D. Wang, Prof. L.-J. Wan
Institute of Chemistry, The Chinese Academy of Sciences
Beijing 100190 (China)
E-mail: wanlijun@iccas.ac.cn

Supporting information for this article is available on the WWW under http://dx.doi.org/10.1002/anie.201303924.

expected to be dominantly synthesized inside MMT because of the spatial confinement. Our results even indicate that the content of the planar pyridinic and pyrrolic N is inversely proportional to the interspace width (δ) of MMT. Electrochemical evaluations showed that the NG synthesized in MMT exhibited excellent electronic conductivity, high ORR activity, and good stability in acidic electrolytes. MMT was previously used to prepare two-dimensional graphite.[14] However, it has thus far not been recognized that MMT can be used to exclude quaternary N during the synthesis of NG and can therefore enable the synthesis of NG with more planar pyridinic and pyrrolic N to catalyze the ORR.

The procedure for the synthesis of NG inside MMT is illustrated in Figure 1. AN monomers were first intercalated into the layers of MMT, and then in situ oxidation polymer-
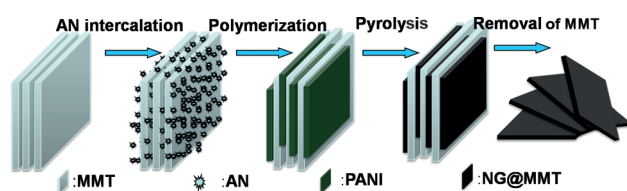

Figure 1. Schematic representation of the synthesis of NG@MMT.

ization was performed. An excess of MMT over AN was used to ensure that most of the AN monomers were intercalated into the layers of MMT and did not remain outside the MMT. The composite was dehydrated at 120°C and then pyrolyzed at 900°C under flowing N_2 for 3 h. Two types of MMT with different interspacial widths, that is, Na-MMT (0.53 nm) and H-MMT (0.46 nm), were used to synthesize NG. The resultant NG samples are accordingly denoted as NG@MMT and NG@H-MMT, respectively. Unless otherwise stated, MMT refers to Na-MMT. For comparison, NC obtained by AN polymerization and pyrolysis without MMT and that obtained from a simple mixture of MMT were termed NC◯MMT and NC⊙MMT, respectively. In the case of NC⊙MMT, AN monomers were not intercalated into the layers of MMT as they were in the case of NG@MMT; rather, they were simply directly mixed with MMT and then polymerized and pyrolyzed to simulate the case of NC formed between MMT particles. The crevice between MMT particles was estimated to be approximately 1 μm. The MMT in all samples was finally etched off in a 40% HF solution.

The procedure for the synthesis of NG@MMT was monitored by X-ray diffraction (XRD). The MMT maintained a well-defined layered structure with a layer distance (d_{001}) of 1.46 nm after polyaniline (PANI) intercalation (see Figure S1a in the Supporting Information). After the pyrolysis step at 900°C, the layer distance of MMT decreased to 1.24 nm, and a graphite peak emerged in the XRD pattern at 27.5° with a d spacing of 0.323 nm (see Figure S1b); this peak was assigned to superposition of the graphene layers. The graphite peak disappeared when MMT was removed because, in this case, no means of restricting the graphene-layer superposition, which resulted in the formation of graphite, was present. Meanwhile, a broad peak appeared at approximately 23.5° in the pattern of the final NG@MMT; this peak

is the graphene (002) diffraction peak (see Figure S1c). The broadness of the peak implies that the NG@MMT is randomly piled in a corrugated structure. The prepared NG@MMT is composed of ultrathin corrugated nanosheets (Figure 2; see also Figure S2). Notably, numerous edge planes appear on the surface of the NG@MMT nanosheets (Figure 2C; see also Figure S2c–e). Previous studies revealed that
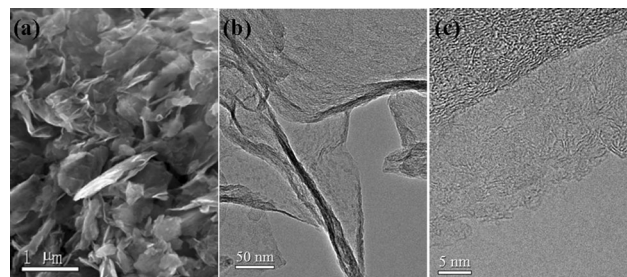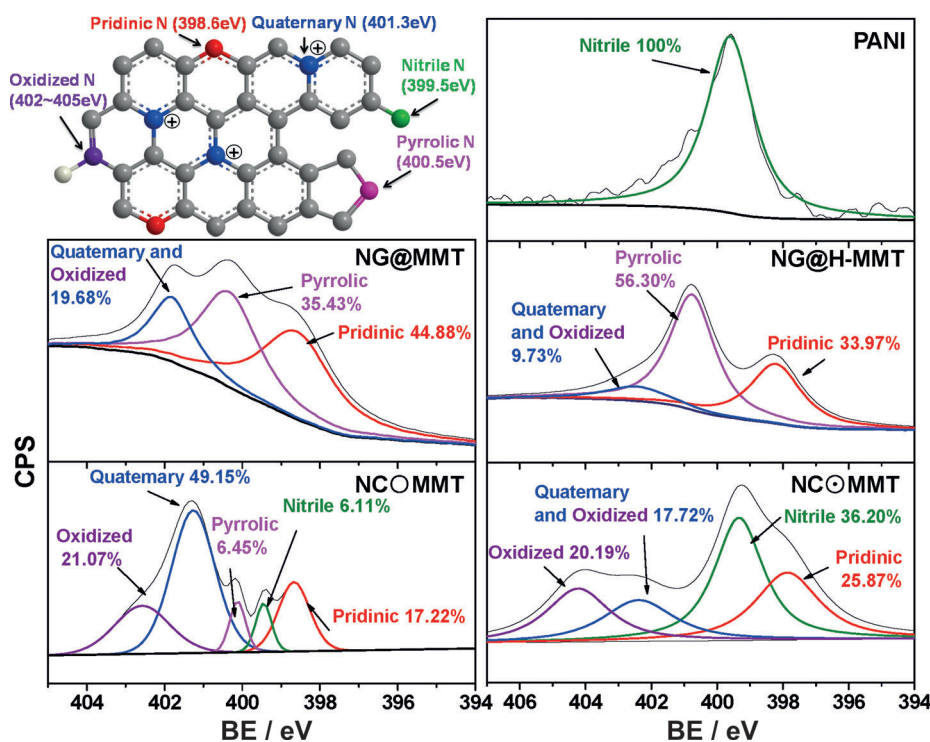

Figure 2. a,b) SEM (a) and TEM images (b) of NG@MMT. c) High-resolution TEM image of the edge of a NG@MMT nanosheet.

nitrogen-containing carbon structures with more exposed edge planes contain more ORR-active nitrogen groups on their surface.[9b] In contrast, the TEM image of NC◯MMT reveals a large-scale spherical morphology (see Figure S3). From the Raman spectra (see Figure S4), the calculated I_G/I_{2D} ratio for the NG@MMT is 1.3, which indicates that the NG@MMT consists of 2–4 layers of graphene (approximately 1.5 nm thick).[15a] This result is identical to those of the AFM (see Figure S2f), which show that the height of an NG@MMT flake is about 1.5–2.5 nm. Notably, the interspace of the MMT (0.53 nm, see Figure S5) only allows the presence of a single layer of graphene; therefore, 2–4 layers of graphene overlap after the MMT has been removed. The weak 2D peak for NC◯MMT implies that NC◯MMT is disordered and different from graphite.[15b]
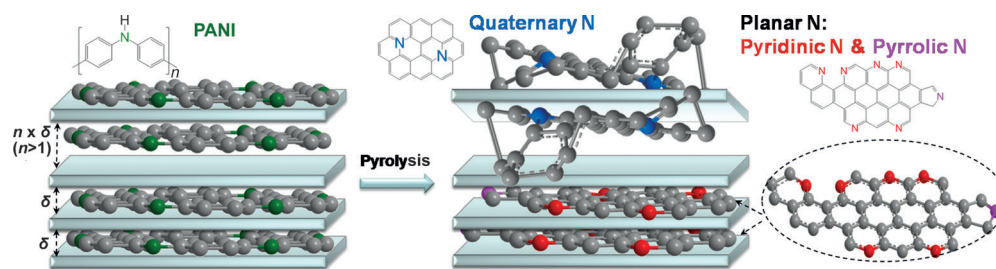
The XPS spectra of the prepared samples clearly indicate the presence of carbon and nitrogen (see Figure S7). The existence of C−N and C−C (graphite-type) bonds in the matrix further confirms the N-doped graphite structure of the prepared samples (see Figure S7b). The relative N/C ratio was only 3.85% in NC◯MMT but was 6.85, 4.22, 4.70, and 4.80% in PANI (before pyrolysis), NG@MMT, NG@H-MMT, and NC⊙MMT, respectively; these ratios indicate that nitrogen loss during pyrolysis at high temperatures was alleviated by the introduction of MMT.

As previously mentioned, pyridinic and pyrrolic N (planar N) are ORR-active catalysts but are unstable at high temperatures, at which quaternary and oxidized N sites would be dominant.[4a,11] More than 70% of the N species in NC◯MMT are oxidized (21.07%) and quaternary (49.15%) N, whereas planar N species only account for 23.67% of the N species (Figure 3). These values are consistent with those previously reported for NC obtained from direct pyrolysis.[4a,6] In contrast, the planar-N content in NG@MMT and NG@H-MMT is as high as 80.32 and 90.27%, respectively, after pyrolysis at 900°C. These data suggest that the active N species, that is, pyridinic N and pyrrolic N species, were produced selectively and were well-preserved inside the interspace of the MMT flat nanoreactor at high temperatures.

Figure 3. N1s XPS spectra of PANI, NG@MMT, NG@H-MMT, NC⊙MMT, and NC○MMT.

with quaternary N is primarily produced in cases in which no MMT is used or in cases in which NG is formed outside the layers of MMT or inside the layers of MMT with a large interspace. Inside the layers of MMT, NG with planar pyridinic and pyrrolic N sites is produced to a very large extent. Because of the torsion angle of the C–N bond, that is, 0° for planar sp^2-hybridized N and 60° for tetrahedral sp^3-hybridized N,[13] graphene with quaternary N forms an uneven structure, whereas graphene with pyridinic and pyrrolic N forms flat platelets. Therefore, the production of graphene with pyridinic N and pyrrolic N is more favorable in a flat nanoreactor than the production of graphene with quaternary N for steric reasons. When the layer distance is decreased further, as in H-MMT, the steric hindrance is further enhanced, and almost no space is left for uneven structure formation. Consequently, NG@H-MMT is doped with a high planar-nitrogen content of 90.27%.

The planar-N content is strongly related to the interspace width of the MMT (Table 1). The yield of planar N species was highest when H-MMT with the smallest interspace width of 0.46 nm was used as a nanoreactor (90.27%) and decreased to 80.32% when MMT with $\delta = 0.53$ nm was used, further to 25.87% when the synthesis was carried out between MMT particles ($\delta \approx 1\ \mu m$), and finally to 23.67% when no MMT was used. The order of the amount of quaternary and oxidized N species produced was reversed. This phenomenon is attributed to the space confinement of the MMT quasi-closed flat nanoreactor. In the case of pyrolysis in MMT with a large δ value, there is no space confinement for NC formation (Figure 4). The incorporation of N occurs randomly at high temperatures, whereby the N atoms preferentially occupy the positions as quaternary N or oxidized N for stability. Thus, NG

formation. Consequently, NG@H-MMT is doped with a high planar-nitrogen content of 90.27%.

Good electrical conductivity is a prime requirement for materials used in electrochemical applications.[6a, 7a] Electrochemical impedance spectroscopy (EIS) performed at high frequency (see the Supporting Information for details) revealed that the electrical resistance of the NG samples was significantly lower than that of the NC samples and similar to that of commercially available Vulcan XC-72R carbon (Figure 5a). These results indicate that the electrical

Figure 4. Schematic representation showing the selectivity inside and outside of MMT during NG synthesis.

Table 1: XPS data and RRDE results for NC○MMT, NC⊙MMT, NG@MMT, and NG@H-MMT.

Sample	Synthesis conditions	δ [nm]	Planar N [%]	Quaternary and oxidized N [%]	Nitrile N [%]	Specific area [$m^2 g^{-1}$]	j_k at 0.7 V [mA cm^{-2}]	H_2O_2 yield [%][a]
NC○MMT	without MMT	∞	23.67	70.22	6.11	171.5	0.1	30.03
NC⊙MMT	between MMT particles	ca. $10^{3[b]}$	25.87	39.91	36.20	226.4	0.3	8.30
NG@MMT	inside Na-MMT	0.56[c]	80.32	19.68	0	247.0	4.6	3.72
NG@H-MMT	inside H-MMT	0.46[c]	90.27	9.73	0	290.3	9.2	2.18

[a] Maximum values. [b] Crevice between MMT particles. [c] Layer-to-layer interspace width of MMT (see Figure S5).

conductivity of the NG samples is as high as that of carbon. The highest electrical conductivity among the different N-doped materials was observed for NG@H-MMT and decreased in the order NG@MMT > NC○MMT > NC⊙MMT. Considered together with the N1s XPS data, the electrical conductivity of these N-doped materials is closely related to the quaternary- and oxidized-N content. The conductivity increases as the quaternary- and oxidized-N content decreases. NG@H-MMT, which had the lowest quaternary- and oxidized-N content, exhibited the highest electrical conductivity. NC⊙MMT is an exception; its low electrical conductivity is attributed to the large number of nitrile species (36.20%).

The electrocatalytic activity of NG@MMT toward the ORR was first examined by linear sweep voltammetry (LSV) at a slow scanning rate of $2\,mV\,s^{-1}$ (see Figure S8). The cathodic current with an onset potential of 0.895 V (versus the reversible hydrogen electrode, RHE) is well-defined in O_2-saturated 0.5 M H_2SO_4; however, it is featureless in N_2-saturated H_2SO_4. It was estimated from the Koutecky–Levich plot that the reaction electron number is 3.8 at 0.55 V versus RHE (see Figure S6b). We further evaluated the activity of the catalysts in rotating ring–disk electrode (RRDE) experiments. All of the RRDE experiments were performed in 0.1 M $HClO_4$ to prevent Pt/C performance loss caused by bisulfate adsorption. The polarization curves for the catalysts are shown in Figure 5b. The NG@H-MMT catalyst exhibited the highest activity. The signal of the half-wave potential on a NG@H-MMT catalyst electrode was only 60 mV less than that on a state-of-the-art carbon-supported platinum catalyst (Johnson Matthey, UK, 40 wt%, denoted as JM Pt/C) at a Pt loading of 25 $\mu g\,Pt\,cm^{-2}$. The H_2O_2 yield was as low as 2.2% at all potentials, whereas the maximum H_2O_2 yield on JM Pt/C was approximately 4.60%, which is consistent with the value of 3–4% reported previously.[16]

Given that the surface nitrogen group is closely related to the ORR activity of NC materials, a comprehensive comparison was made on the basis of high-resolution N1s XPS data combined with the results of the RRDE experiments. The results clearly indicate that the incorporation of planar nitrogen into materials plays an important role in the ORR process (Table 1). The kinetic current densities (j_k) were maximized for NG@H-MMT and decreased in the order NG@MMT > NC⊙MMT > NC○MMT, with j_k values of 9.2, 4.6, 0.3, and 0.1 $mA\,cm^{-2}$, respectively, at 0.7 V. The same order of planar-N ratios was observed for these samples; that is, NG@H-MMT (90.27%) > NG@MMT (80.32%) > NC⊙MMT (25.87%) > NC○MMT (23.67%). The ORR activities of these N-doped materials increased as their planar-N content increased.

The Brunauer–Emmet–Teller (BET) specific surface areas of NC○MMT, NC⊙MMT, NG@MMT, and NG@H-MMT are 171.55, 226.39, 247.01 and 290.27 $m^2\,g^{-1}$, respectively (see Figure S9). The specific activities normalized with respect to the specific surface areas of the samples are 0.97, 2.21, 31.04 and 52.82 $mA\,m^{-2}$, accordingly (see Figure S10). These results indicate that the specific activity strongly depends on the catalyst type rather than the BET specific surface area. The major reason for the activity enhancement is
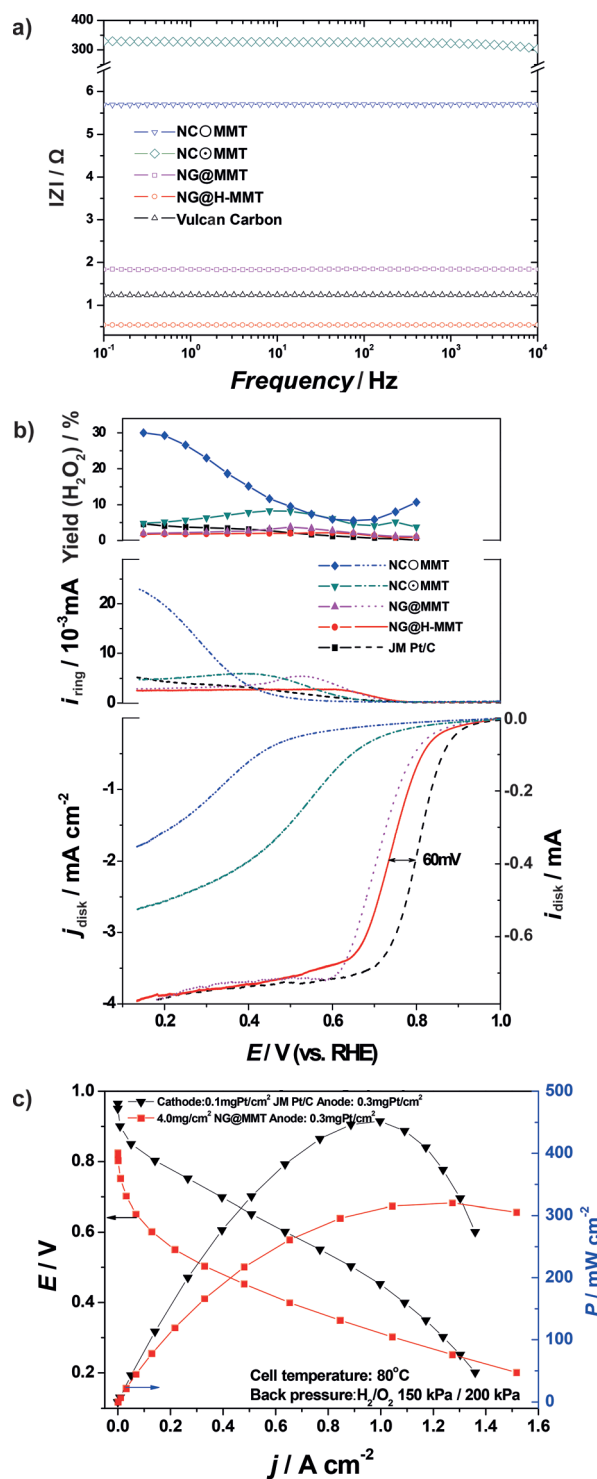
Figure 5. a) Bode spectra obtained through the application of a sine wave with an amplitude of 5.0 mV from 10 mHz to 10 kHz for different catalysts. b) Steady-state plots of ORR polarization (bottom), ring current (middle), and H_2O_2 yield (top) for different catalysts in O_2-saturated 0.1 M $HClO_4$. c) Polarization curves and corresponding power densities of membrane electrode assemblies fabricated with the NG@MMT cathode catalyst.

the density of surface active sites rather than the total surface area, although the importance of the specific surface area cannot be ruled out totally.

Although the NG@MMT catalysts exhibited relatively high ORR activities, their stability is a prominent concern. We evaluated the stability of the NG@MMT catalysts by cycling the electrode not only in the potential range of 0.6–1.1 V in O_2-saturated 0.1 M $HClO_4$ but also in a larger potential range of 0–1.2 V in N_2-saturated 0.5 M H_2SO_4 (see Figure S11). No noticeable change in the ORR catalytic activity was observed for the NG@MMT. In contrast, the ORR half-wave potential on the electrode prepared from JM Pt/C catalysts was negatively shifted by 22 mV after O_2 cycling and negatively shifted by 73 mV after N_2 cycling. Besides, the NG@MMT exhibited high selectivity toward the ORR with a remarkable tolerance for methanol (see in Figure S12).

The performance of the single cell with the NG@MMT cathode catalyst and the state-of-the-art Pt/C cathode catalyst at a Pt loading of 0.1 mg cm^{-2} is shown in Figure 5c. The maximum power output was 320 mW cm^{-2} for the NG@MMT and 451 mW cm^{-2} for Pt/C. Notably, no metal, let alone a precious metal, was present in the NG@MMT sample. We believe that the performance of these NG catalysts can be further improved by enhancing oxygen transport in the catalytic layer, as Dodelet and co-workers did. Dodelet and co-workers developed a catalyst based on Fe and a metal–organic framework with an impressive volumetric activity of 230 A cm^{-3} at 0.8 V$_{iR-free}$.[1d,e] Although some catalysts prepared with Fe and/or Co present showed similar or even better single-cell performance and ORR activity,[1] no metal-free catalyst with such high activity in acidic environments has been reported previously.

In summary, we have fabricated NG by a novel approach with the aid of MMT, which is an inexpensive flat nanoreactor for the fabrication of nanosheet materials. Planar N sites, which are catalytically active toward the ORR, were generated selectively with the flat nanoreactor. The selectivity for planar N strongly depends on the interspace width of the flat nanoreactor. The highest yield of planar N (90.3%) was observed when H-MMT, with an interspace width of 0.46 nm, was used as a nanoreactor. The content of quaternary and oxidized N was restricted to less than 9.7% because of steric hindrance. The prepared NG showed good N incorporation, excellent electronic conductivity, and good catalytic activity toward the ORR. This synthetic method avoids vacuum-based, elaborate procedures and thus provides a simple but efficient and versatile approach to the low-cost mass production of NG for industrial purposes that range from catalysis and sensors to supercapacitors and lithium-ion batteries.

[1] a) K. P. Gong, F. Du, Z. H. Xia, M. Durstock, L. M. Dai, *Science* **2009**, *323*, 760; b) M. Lefevre, E. Proietti, F. Jaouen, J. P. Dodelet, *Science* **2009**, *324*, 71; c) G. Wu, K. L. More, C. M. Johnston, P. Zelenay, *Science* **2011**, *332*, 443; d) J. Tian, A. Morozan, M. T. Sougrati, M. Lefèvre, R. Chenitz, J.-P. Dodelet, D. Jones, F. Jaouen, *Angew. Chem.* **2013**, *125*, 7005; *Angew. Chem. Int. Ed.* **2013**, *52*, 6867; e) E. Proietti, F. Jaouen, M. Lefèvre, N. Larouche, J. Tian, J. Herranz, J.-P. Dodelet, *Nat. Commun.* **2011**, *2*, 416.

[2] Z. D. Wei, S. T. Zhang, Z. Y. Tang, H. T. Gou, *J. Appl. Electrochem.* **2000**, *30*, 723.

[3] a) X. Huang, Z. Y. Yin, S. X. Wu, X. Y. Qi, Q. Y. He, Q. C. Zhang, Q. Y. Yan, F. Boey, H. Zhang, *Small* **2011**, *7*, 1876; b) Q. Y. He, S. X. Wu, Z.-Y. Yin, H. Zhang, *Chem. Sci.* **2012**, *3*, 1764; c) X. Huang, X.-Y. Qi, F. Boey, H. Zhang, *Chem. Soc. Rev.* **2012**, *41*, 666; d) X. Huang, Z. Zeng, Z. Fan, J. Liu, H. Zhang, *Adv. Mater.* **2012**, *24*, 5979.

[4] a) D. S. Yu, Q. Zhang, L. M. Dai, *J. Am. Chem. Soc.* **2010**, *132*, 15127; b) L. Qu, Y. Liu, J.-B. Baek, L. Dai, *ACS Nano* **2010**, *4*, 1321; c) Y. F. Tang, B. L. Allen, D. R. Kauffman, A. Star, *J. Am. Chem. Soc.* **2009**, *131*, 13200.

[5] Y. Zhao, L.-J. Yang, S. Chen, X.-Z. Wang, Y.-W. Ma, Q. Wu, Y.-F. Jiang, W.-J. Qian, Z. Hu, *J. Am. Chem. Soc.* **2013**, *135*, 1201.

[6] a) R. L. Liu, D. Q. Wu, X. L. Feng, K. Müllen, *Angew. Chem.* **2010**, *122*, 2619; *Angew. Chem. Int. Ed.* **2010**, *49*, 2565; b) W. Yang, T. P. Fellinger, M. Antonietti, *J. Am. Chem. Soc.* **2011**, *133*, 206.

[7] a) R. A. Sidik, A. B. Anderson, N. P. Subramanian, S. P. Kumaraguru, B. N. Popov, *J. Phys. Chem. B* **2006**, *110*, 1787; b) G. Liu, X. G. Li, J. W. Lee, B. N. Popov, *Catal. Sci. Technol.* **2011**, *1*, 207; c) Y. Liang, Y. Li, H. Wang, J. Zhou, J. Wang, T. Regier, H. Dai, *Nat. Mater.* **2011**, *10*, 780; d) S. Wang, L. Zhang, Z. Xia, A. Roy, D.-W. Chang, J.-B. Baek, L. Dai, *Angew. Chem.* **2012**, *124*, 4285; *Angew. Chem. Int. Ed.* **2012**, *51*, 4209.

[8] a) B. Guo, Q. Liu, E. Chen, H. Zhu, L. Fang, J.-R. Gong, *Nano Lett.* **2010**, *10*, 4975; b) D. Geng, Y. Chen, Y. Li, R. Li, X. Sun, S. Ye, S. Knights, *Energy Environ. Sci.* **2011**, *4*, 760; c) D. Wei, Y. Liu, Y. Wang, H. L. Zhang, G. Yu. Huang, *Nano Lett.* **2009**, *9*, 1752.

[9] a) Z.-J. Wang, R.-R. Jia, J.-F. Zheng, J.-H. Zhao, L. Li, J.-L. Song, Z.-P. Zhu, *ACS Nano* **2011**, *5*, 1677; b) P.-H. Matter, E. Wang, M. Arias, E.-J. Biddinger, U.-S. Ozkan, *J. Phys. Chem. B* **2006**, *110*, 18374.

[10] a) J. Zhao, G.-Y. Zhu, W. Huang, Z. He, X.-M. Feng, Y.-W. Ma, X. C. Dong, Q.-L. Fan, L.-H. Wang, Z. Hu, Y.-N. Lu, W. J. Huang, *Mater. Chem.* **2012**, *22*, 19679; b) H. Chen, Y. Yang, Z. Hu, K.-F. Huo, Y.-W. Ma, Y. Chen, *J. Phys. Chem. B* **2006**, *110*, 16422.

[11] a) S.-B. Yang, X.-L. Feng, X.-C. Wang, K. Müllen, *Angew. Chem.* **2011**, *123*, 5451; *Angew. Chem. Int. Ed.* **2011**, *50*, 5339; b) C.-V. Rao, C.-R. Cabrera, Y. Ishikawa, *J. Phys. Chem. Lett.* **2010**, *1*, 2622.

[12] a) X. B. Wang, Y. Q. Liu, D. B. Zhu, L. Zhang, H. Z. Ma, N. Yao, B. L. Zhang, *J. Phys. Chem. B* **2002**, *106*, 2186; b) J. Casanovas, J. M. Ricart, J. Rubio, F. Illas, J. M. Jiménez-Mateos, *J. Am. Chem. Soc.* **1996**, *118*, 8071; c) T. B. Martins, R. H. Miwa, A. J. Silva, R. A. Fazzio, *Phys. Rev. Lett.* **2007**, *98*, 196803.

[13] G. Gastone, B. Valerio, B. Fabrizio, F. Valeria, *J. Am. Chem. Soc.* **1986**, *108*, 2420.

[14] a) N. Sonobe, T. Kyotani, A. Tomita, *Carbon* **1990**, *28*, 483; b) T. Kyotani, A. Tomita, *Ceramics* **1991**, *26*, 573.

[15] a) A. Reina, X.-T. Jia, J. Ho, D. Nezich, H. B. Son, V. Bulovic, M. S. Dresselhaus, J. Kong, *Nano Lett.* **2009**, *9*, 30; b) H.-J. Scheibe, D. Drescher, P. Alers, *Fresenius J. Anal. Chem.* **1995**, *353*, 695.

[16] M. Inaba, H. Yamada, J. Tokunaga, A. Tasaka, *Electrochem. Solid-State Lett.* **2004**, *7*, A474.